

1 **Manuscript type: Article - Discovery**

2

3 **Conflicting evolutionary histories of the mitochondrial and nuclear genomes in New World *Myotis***

4 Roy N. Platt¹, Brant C. Faircloth², Kevin A.M. Sullivan¹, Troy Kieran³, Travis C. Glenn³, Michael W.
5 Vandewege¹, Tom E. Lee⁴, Robert J. Baker¹, Richard D. Stevens⁵, David A. Ray^{1*}

6

7 ¹ Department of Biological Sciences, Texas Tech University, Lubbock, USA

8 ² Department of Biological Sciences and Museum of Natural Science, Louisiana State University, Baton
9 Rouge, USA

10 ³ Environmental Health Science, University of Georgia, Athens, USA

11 ⁴ Department of Biology, Abilene Christian University, Abilene, USA

12 ⁵ Natural Resource Management, Texas Tech University, Lubbock, USA

13

14 *Corresponding author: E-mail: david.4.ray@gmail.com

15

16 **Abstract**

17 The diversification of *Myotis* into more than 100 species in just a few million years is one of the
18 most extensive mammalian radiations available for study. Efforts to understand relationships within
19 *Myotis* have primarily utilized mitochondrial markers, and trees inferred from nuclear markers lacked
20 resolution. Our current understanding of relationships within *Myotis* is therefore biased towards a set of
21 phylogenetic markers that may not reflect the phylogenetic history of the nuclear genome. To resolve
22 this, we sequenced the full mitochondrial genomes of 37 representative *Myotis*, primarily from the New
23 World, in conjunction with targeted sequencing of 3,648 ultraconserved elements (UCEs). We inferred the
24 phylogeny of *Myotis* and explored the effects of concatenation and summary phylogenetic methods, as
25 well as combinations of markers based on informativeness or levels of missing data, on our phylogenetic
26 results. Of the 295 phylogenies generated from the nuclear UCE data, all are significantly different from
27 phylogenies inferred using mitochondrial genomes. Even within the nuclear genome quartet frequencies
28 indicate that around half of all UCE loci conflict with the estimated species tree. Several factors can drive
29 such conflict, including incomplete lineage sorting, introgressive hybridization, or even phylogenetic error.
30 Despite the degree of discordance between nuclear UCE loci and the mitochondrial genome and among
31 UCE loci themselves, the most common nuclear topology is recovered in one quarter of all analyses with

32 strong nodal support. Based on these results, we re-examine the evolutionary history of *Myotis* to better
33 understand the phenomena driving their unique nuclear, mitochondrial, and biogeographic histories.

34

35 **Keywords**

36 incomplete lineage sorting, summary tree methods, concatenation, Vespertilionidae, phylogenomics,
37 UCE, ultraconserved elements, reticulation

38

39 Introduction

40 The genus *Myotis* (Order Chiroptera, Family Vespertilionidae) contains more than 100 species that
41 originated during the last 10-15 million years (Stadelmann, et al. 2007), making it one of the most
42 successful, extant, mammalian species radiations. Members of *Myotis* are distributed worldwide,
43 excluding polar regions, and generally share a similar ecological niche: aerial insectivory. *Myotis* species
44 often exhibit little morphological differentiation and, as a result, the rate of cryptic speciation within the
45 genus is thought to be high. For example, specimens identified as *M. nigricans* and *M. albescens* form
46 multiple paraphyletic lineages distributed throughout the phylogeny of Neotropical *Myotis* (Larsen, et al.
47 2012).

48 Confounding matters, the morphological variation that exists is often a poor indicator of species-
49 level relationships. Early classifications of *Myotis* identified three major morphotypes (Findley 1972); each
50 were assumed to be monophyletic and were recognized at the subgeneric level (Simmons 2005).
51 Subsequent phylogenetic analyses of the mitochondrial cytochrome-b (*cytb*) gene recovered paraphyletic
52 origins of the morphologically defined subgenera, suggesting convergent evolution in *Myotis* (Ruedi and
53 Mayer 2001). These same analyses demonstrated that geography was a better predictor of phylogenetic
54 relationship than morphology (Ruedi and Mayer 2001; Stadelmann, et al. 2007). Generally, *Myotis*
55 phylogenies from mitochondrial data contain a single bifurcation at the base of the tree that splits Old
56 World from New World species. An additional bifurcation within New World species separates Nearctic
57 (NA) from Neotropical (NT) species. The NA/NT bifurcation is not absolute, with at least five NA species
58 located in the Neotropics and *vice versa*. The Old World/New World bifurcation is stricter, with only two
59 Old World species, *M. brandtii* and *M. gracilis*, present in the New World clade.

60 The ability of mitochondrial markers to resolve a well-supported topology does not guarantee
61 that the mitochondrial tree represents the species tree (for examples see Willis, et al. 2014; Li, et al. 2016;
62 Leavitt, et al. 2017). Despite containing 37 genes, the lack of recombination and uniparental inheritance
63 of the mitochondrion means that it is transmitted as a single genetic unit. This makes mitochondria
64 susceptible to evolutionary processes that may cause its history to diverge from the history of the species
65 (Edwards and Bensch 2009). The most widely accepted phylogenies of *Myotis* rely heavily on
66 mitochondrial data and even phylogenies containing nuclear data demonstrate an over reliance on
67 mitochondrial markers for resolution. For example alignments of the nuclear *RAG2* and mitochondrial
68 *cytb* contained 162 and 560 variable characters respectively (Stadelmann, et al. 2007). Phylogenetic
69 analyses of *RAG2* in *Myotis* results in a tree primarily composed of polytomies (Stadelmann, et al. 2007).
70 Combining these two markers increases phylogenetic resolution, but the results are heavily influenced by

71 larger numbers of mitochondrial characters, potentially masking signal from the nuclear marker
72 (Stadelmann, et al. 2007; Larsen, et al. 2012; Ruedi, et al. 2013; Haynie, et al. 2016).

73 It is difficult to draw major conclusions from studies limited in the number of characters (Ruedi
74 and Mayer 2001; Stadelmann, et al. 2007; Larsen, et al. 2012; Ruedi, et al. 2013; Haynie, et al. 2016) or
75 taxa (Platt, et al. 2015). Current data seem to indicate that nuclear and mitochondrial markers recover
76 similar topologies. Platt et al. (2015) generated a phylogeny based entirely on nuclear data using 85,028
77 shared transposable element insertions. Their results generally confirmed the mitochondrial phylogenies
78 of *Myotis*, but only included seven taxa in their analysis. In order to fully resolve relationships and
79 understand the *Myotis* radiation it is necessary to increase character and taxon sampling.

80 Recently, targeted sequencing methods have been developed that utilize baits to enrich and
81 sequence ultraconserved elements (UCEs; Faircloth, et al. 2012), and this method has resolved a number
82 of difficult phylogenetic problems (for examples see Crawford, et al. 2012; McCormack, et al. 2013; Green,
83 et al. 2014; Faircloth, et al. 2015; McGee, et al. 2016). Generally speaking, the conserved “core” of UCE
84 regions allows thousands of homologous loci to be enriched from divergent organismal genomes while
85 the sequence that flanks the core UCE region contains a majority of phylogenetically informative sites –
86 allowing researchers to collect a large number of phylogenetically informative, homologous loci from
87 throughout the genome in a cost-effective and efficient manner. Broad sampling of the nuclear genome
88 should help to resolve a phylogeny without an over reliance on mitochondrial loci. In addition, increasing
89 the number of nuclear loci sampled from a handful of genes to thousands can recover accurate trees
90 despite high levels of incomplete lineage sorting (Maddison and Knowles 2006)

91 Here, we used targeted sequencing of UCEs to collect ~1.4 Mbp from $\geq 3,600$ nuclear loci in 37
92 taxa, primarily representing New World *Myotis*. Combinations of the UCE data were analyzed using
93 concatenation and tree summary methods to estimate the *Myotis* phylogeny. Analysis of the nuclear UCE
94 data recovered 295 trees representing 175 distinct topologies. The nuclear topologies were compared to
95 trees generated from full mitochondrial genomes to test for conflict between the two types of markers.
96 Our results show that, despite the range of trees recovered from the nuclear data, nuclear and
97 mitochondrial markers always depict conflicting phylogenies. Given that the nuclear and mitochondrial
98 trees are distinct from one another it is necessary to reinvestigate conclusions made based solely on the
99 mitochondrial phylogeny.

100

101 **Results**

102 We used targeted sequencing of UCEs to collect sequence data from 3,648 nuclear loci which we
103 assembled into concatenated alignments as large as 1.37 Mb. In addition, we assembled mitochondrial
104 genomes for most taxa. We then used the data to infer the phylogenetic history of New World *Myotis* in
105 three phases: UCE and mitogenome assembly, initial phylogenetic analysis, extended phylogenetic
106 analyses.

107 UCE and mitochondrial assembly and alignment – We averaged 3.29 million reads per sample
108 after demultiplexing. These reads were assembled into an average of 5,778 contigs per sample (min =
109 1,562 *M. martiniquensis*, max = 11,784 *M. nigricans* 3). Recovery of UCE loci varied across taxa. Of the
110 5,500 loci in the Amniote probe set, we successfully recovered 3,898 UCE loci, 3,648 loci from five or more
111 samples, 212 loci in all 37 samples (Table 2). On average, 3,332 UCE loci were recovered per sample,
112 ranging from 1,106 (*M. martiniquensis*) 4,008 (*M. keaysi*). Repetitive sequences, identified via
113 RepeatMasker searches, were minimal occupying less than 0.02% of sites across all UCE alignments.
114 Sequence coverage of the mitochondrial genomes averaged 58x (range >1x - 297x). Mitochondrial
115 genome assemblies varied in quality. Some were almost entirely complete while others were missing
116 sections. We found three premature stop codons in mtDNA protein coding genes. Subsequent manual
117 alignment and validation suggested that these regions were miscalled by MitoBim, and we corrected the
118 errors prior to analysis.

119 Initial phylogenetic analyses – Initial analysis of the nuclear data used loci that were present in 20
120 or more taxa. This resulted in an alignment of 1,144,471 bp from 2,890 nuclear loci containing 35,284
121 parsimony informative characters. The 2,890 loci were split into 27 partitions as recommended by
122 PartitionFinder (Lanfear, et al. 2012). Maximum likelihood and Bayesian analyses recovered the same
123 topology and found similar support for most nodes (Figure 1A). Maximum likelihood analysis recovered
124 100% support for 31 of 35 bipartitions, and 33 bipartitions were present in $\geq 98\%$ bootstrap replicates.
125 Nodes with the least support were still present in 86% - 88% of bootstrap replicates. After 50 bootstrap
126 replicates the average weighted Robinson-Foulds distance between replicate sets was less than 0.23%
127 (Pattengale, et al. 2009). Bayesian analysis recovered an identical topology, with the only difference being
128 that all bipartitions were supported with a clade probability value of >0.99 . Visual inspection of the
129 parameter files in Tracer v1.6 showed good sampling with a likelihood score of -2.419×10^{-6} and an
130 effective sample size (ESS) of 637 for the likelihood parameter. All other parameters had effective sample
131 sizes greater than 500. The average standard deviation of split frequencies (ASDF) across all runs was less
132 than 1% after 5,000 generations.

133 Thirty-seven mitochondrial protein coding, rRNA and tRNA genes were concatenated into single
134 alignment of 15,520 bp containing 5,007 informative characters. Alignments for 30 samples were $\geq 90\%$
135 complete, and alignments for five samples were 68-84% complete. Only 21% and 50% of nucleotide
136 positions were present in the *M. albescens*³ (TK 61766) and *Myotis levis* alignments. Maximum likelihood
137 and Bayesian analyses of the mitochondrial data recovered similar topologies (Figure 1B), varying in the
138 *M. thysanodes*, *M. evotis*, and *M. keeni* relationships. Neither method recovered significant support for
139 these relationships. Bootstrap replicates of the maximum likelihood analysis meet the stopping criterion
140 after the first 50 of 10,000 replicates (average weighted Robinson-Foulds value = 2.28%). The RAxML
141 mitochondrial phylogeny was well supported with 29 of 35 nodes present in $\geq 96\%$ of bootstrap replicates.
142 The remaining six nodes were present in 47% to 70% of bootstrap replicates. Bayesian analysis of the
143 mitochondrial data reached convergence, defined as an ASDF of $<1\%$, after the first 424,500 of one million
144 generations. The final ASDF, after discarding 25% of samples, was 0.49%. The trace files from all four
145 independent runs shows proper mixing of samples and the effective sample size for all parameters was
146 greater than 200. The log likelihood score for the Bayesian mitochondrial tree was -1.205×10^{-5} with an ESS
147 of 1,446. In all, posterior probabilities were lower than the bound established as significant (≥ 0.95) for
148 five nodes.

149 Mitochondrial and nuclear analyses recovered different topologies (Figure 1). We stripped branch
150 lengths from all trees and compared the topologies using an approximately unbiased test to determine
151 whether differences in the tree represented conflicting signals in the marker sets. When the nuclear data
152 is constrained to the mitochondrial tree (p -value = 1×10^{-66}) or *vice versa* (p -value = 2×10^{-5}), likelihood
153 scores are significantly worse than expected given similar evolutionary histories. These results reject the
154 hypothesis that the mitochondrial and nuclear UCE phylogenies reflect similar evolutionary histories.

155 Extended phylogenetic analyses - Many factors can bias phylogenetic analyses resulting in inaccurate trees
156 (Sanderson and Shaffer 2002). Rather than assuming our initial nuclear UCE tree was an accurate estimate
157 of the phylogenetic relationships of *Myotis*, we wanted to build a range of plausible topologies from the
158 nuclear UCE data. To do this we reanalyzed the nuclear UCE data set with minor deviations in locus
159 sampling, partitioning, inference method, *etc.* In all this effort resulted in 291 unique phylogenetic
160 analyses. Individual results or topologies are not the focus of these analyses. Rather, the goal was to
161 recover as many, reasonable, nuclear UCE topologies as possible in an effort to account for phylogenetic
162 uncertainty not present in the initial analysis and to compare the range of nuclear UCE trees to the
163 mitochondrial genome tree.

164 We investigated the effects of matrix composition (or completeness) on our phylogenetic
165 inference by generating 10 different alignments having levels of matrix completeness spanning 15-95% at
166 10% intervals and including a final matrix of 100% completeness. Loci in these alignments were partitioned
167 using three separate schemes: all loci were partitioned individually, loci were unpartitioned, or loci were
168 combined into optimum partitions using PartitionFinder. The result was 10 different alignments with three
169 partitioning schemes each. These were analyzed using Bayesian and maximum likelihood methods. Due
170 to computational limits we abandoned the fully partitioned, Bayesian analyses. The length, number of
171 loci, and optimum number of partitions per alignment is shown in Table 2. Bootstrap topologies stabilized
172 in 9 of 10 alignments after 50 replicates and all Bayesian runs converged in less than ten thousand
173 generations. In general, the same alignment produced the same topology regardless of inference method
174 or partitioning scheme with the only exception being the terminal relationships *M. levis*/*M. albescens*
175 clade in the optimum vs. unpartitioned Bayesian analysis of the 100% complete data matrix.

176 Trees were generated from data matrices incorporating loci of differing lengths (Hosner, et al.
177 2016). All 3,648 loci were ordered based on their length and split into nine bins of 365 loci and 1 bin of
178 363 loci, so that the first bin contained the 365 shortest loci, the second bin contained the 366th to the
179 731st, and so on. The number of informative characters per bin ranged from 1,115 to 6,995 and the
180 number of informative characters was correlated with average locus length (Supplemental Figure 2). On
181 average, only 2.6% of characters in each bin were parsimony-informative. Each of the ten length-based
182 alignments recovered slightly different topologies. Terminal relationships were generally stable across
183 analyses with the majority of differences between topologies found in the early bifurcations of the ingroup
184 (*Myotis*).

185 From the above analyses combining different matrix composition, inference method, partitioning,
186 and locus-length variants we observed that, in general, larger alignments produced well resolved
187 topologies with significant nodal support regardless of the phylogenetic method or partitioning scheme
188 used. On the other hand, re-analyses of smaller portions of the data were more likely to recover unique
189 topologies. Given that the overall goal of the extended analyses was to generate as many reasonable
190 nuclear UCE based topologies for comparison with the mitochondrial tree, we decided to randomly
191 sample small portions of the nuclear UCE loci to create alignments that are more likely to result in unique
192 topologies. We randomly subsampled the 3,648 enriched loci to create 100 unique data sets. Loci were
193 concatenated in each replicate data set and analyzed using maximum likelihood in RAxML. Of the 100
194 alignments analyzed, 80 unique topologies were generated (mean Robinson-Foulds distance = 4.3).

195 In addition to concatenated analyses, three summary-based species tree programs were used on
196 datasets of varying matrix-completeness (ASTRAL-II, ASTRID, SVDquartets). Normalized quartet scores
197 from ASTRAL-II (Mirarab and Warnow 2015) analyses were quite consistent with scores ranging from
198 0.540 to 0.553, and between 7,745,739 (100% complete 212 gene trees) and 63,042,410 (15% 3648 loci)
199 induced quartet gene trees. SVDquartets (Chifman and Kubatko 2014) sampled all 66,045 quartets. On
200 average, the total weight of incompatible quartets was 2.84%. Similar to the concatenated analysis, we
201 inferred coalescent-based species from the same 100 subsamples of 365 loci described above. Despite
202 being generated from the same underlying data, summary and concatenation methods only recovered
203 the same tree in one of 100 attempts.

204 Finally, we used weighted and unweighted statistical binning to combine individual gene trees
205 into supergenes, estimate the supergene phylogeny, and then infer the species tree from the supergene
206 trees. The 3,648 loci were combined into 528 binned loci with 480 bins containing seven loci each and 48
207 bins containing six loci each. Normalized quartet scores were 0.672 for the binned-unweighted and 0.673
208 for the binned-weighted ASTRAL-II analysis. Given the relative even distribution of loci into bins the
209 negligible difference in quartet/species tree discordance is expected. Both binning methods recovered
210 the same topology which was the same tree recovered in the initial nuclear UCE analyses and was the
211 most common topology observed across all analyses.

212 Topology comparisons – After rejecting topological congruence between the initial nuclear UCE
213 and mitochondrial phylogenies we used various methods to re-analyze the nuclear UCE data in an effort
214 to identify alternative nuclear topologies. Topological congruence between the mitochondrial sequence
215 data and nuclear topologies resulting from the extended analyses were tested to see if any were
216 statistically congruent with the mitochondrial phylogeny of *Myotis*. Site-log likelihood scores for the
217 mitochondrial alignments when constrained to all 175 unique nuclear UCE topologies were generated in
218 RAxML and analyzed in Consel using the Shimodaira-Hasegawa (Shimodaira and Hasegawa 1999) and
219 approximately unbiased tests (Shimodaira 2002). In each case, the mitochondrial data produced
220 significantly worse likelihood scores, rejecting congruence between the nuclear UCE and mitochondrial
221 phylogenies (Supplemental Table 1).

222 When visualizing all topologies in tree space, nuclear trees co-localized and were distinct from
223 mitochondrial topologies (Figure 2A). Pairwise comparisons of Robinson-Foulds symmetrical differences
224 show that 98.75% of nuclear UCE vs. nuclear UCE (Figure 2B) trees are more similar to each other than
225 the mitochondrial trees are to even the most similar nuclear UCE tree (Figure 2C). The most frequently
226 observed topology was recovered in 45 of the 294 nuclear analyses and was identical to the tree recovered

227 in the initial nuclear UCE analysis (Figure 1a). Of the 45 analyses that recovered the most frequently
228 observed topology, 38 were Bayesian and RAxML searches that varied by matrix completeness and
229 partitioning scheme. The fact that these analyses recovered the same topology is expected given that they
230 are not independent. For example, a RAxML analysis of the 15% complete data set uses 1.26 Mb of the
231 1.38 Mb of data from the 25% complete dataset. These two alignments are 91% identical. Analyses that
232 directly varied the alignments and/or sampled less data (e.g. randomly sampling loci) were more likely to
233 generate unique topologies than the nested analyses described above. Of the 200 analyses that randomly
234 sampled UCE loci 164 unique topologies were observed. This implies that when analyses of large data sets
235 produce well-resolved trees with significant nodal support, sampling smaller portions of the data, may
236 provide a mechanism for creating phylogenetic uncertainty not represented by typical tree scoring
237 metrics. To account for the phylogenetic uncertainty present in our dataset, we generated a consensus
238 tree from all nuclear topologies using an 85% threshold to resolve bipartitions (Figure 3).

239 **Discussion**

240 We generated phylogenies from 3,648 UCE loci and mitochondrial genomes of 35 *Myotis* bats.
241 Initial analyses of the mitochondrial and nuclear UCE phylogenies recovered distinct topologies (Figure 1).
242 Rather than rejecting concordance between the two data types from a single analysis we took steps to re-
243 analyze the nuclear UCE data in an effort to generate as many viable nuclear topologies as possible. We
244 recovered 175 unique nuclear topologies using multiple methodologies, sampling strategies, and
245 parameters. None of these nuclear topologies were similar to the topology produced from the
246 mitochondrial data suggesting that nuclear UCE loci and the mitochondrial genomes of *Myotis* have
247 distinct evolutionary histories. The conflict between the mitochondrial and nuclear data may be driven by
248 error in phylogenetic estimation or may reflect genuine conflict between the two marker types (Degnan
249 and Rosenberg 2009; Huang, et al. 2010). We relied on multiple tree-inference methods (e.g. summary
250 vs. concatenation), manipulated phylogenetic parameters (e.g. partitioning strategy), and sampling
251 criteria (e.g. loci sampled in all taxa) to minimize the impacts of phylogenetic error on the data set. In most
252 cases, varying parameter or methodologies generated unique topologies, often due to rearrangements of
253 a few terminal taxa. *M. volans* and *M. brandtii* were often placed as either sister to the remaining NW
254 *Myotis* or as an early bifurcation between the NA and NT clades. *M. vivesi* was often found as sister to the
255 clade containing *M. lucifugus*, *occultus* and *fortidens* or as sister to the clade containing the NT *Myotis*.

256 Around 98.3% of all nuclear tree vs. nuclear tree comparisons contain fewer than 30 symmetric
257 differences (Figure 2b) but there are no mitochondrial vs. nuclear tree comparisons with less than 30
258 symmetric differences (Figure 2c). Interestingly, the most common nuclear topology most often recovered

259 by concatenation analyses (Figure 1A). Summary methods failed to recover the most common nuclear
260 topology except when loci were binned together prior to gene tree estimation. Summary methods also
261 tended to recover more unique topologies than concatenation methods when analyzing data from the
262 same gene(s). For example, the random sample analyses recovered 80 unique topologies using
263 concatenation (RAxML) and 89 unique topologies with summary methods (ASTRAL-II). This likely has to
264 do with the limited number of informative characters per locus and by extension limited phylogenetic
265 signal per gene tree (Supplemental Figure 2). In these instances, limited phylogenetic signal per gene
266 would likely lead to increased opportunity for phylogenetic error in gene tree estimation. Further
267 supporting this idea, binning of compatible UCE loci may have indirectly increased phylogenetic signal
268 resulting in the same topology that many of the concatenation analyses recovered. No other
269 summary/coalescent method recovered this topology.

270 Previous work with UCE loci demonstrated that support for deep divergences varied based on the
271 number of loci examined (McCormack, et al. 2013). Further, bootstrap replicates and clade probability
272 values can be inaccurate metrics of nodal support (Douady, et al. 2003; Hedtke, et al. 2006). Varying the
273 input data and phylogenetic parameters can produce a range of reasonable nuclear topologies that may
274 be more useful than overreliance on a tree resulting from a one or two analyses. Here, by considering the
275 different topologies that result from various analyses (e.g. partitioning strategies, inference methods,
276 etc.), we can account for phylogenetic uncertainty better than considering a single nuclear or
277 mitochondrial topology alone.

278 The mitochondrial alignment constrained to any of the 175 nuclear topologies generated
279 significantly worse likelihood scores than expected by chance (Supplemental Table 2) and a comparison
280 of topologies in tree space shows that the mitochondrial topologies are unique from all nuclear topologies
281 (Figure 2A). Pairwise tree distances demonstrate that all but the most divergent nuclear topologies are
282 more similar to each other (Figure 2B) than any nuclear vs. mitochondrial comparison (Figure 2C). Despite
283 the number of different analyses, the nuclear data never recover a topology that is similar, much less
284 identical, to the mitochondrial topology.

285 Multiple studies have recovered effectively the same relationships among *Myotis* using
286 mitochondrial markers to the one presented here (Ruedi and Mayer 2001; Stadelmann, et al. 2007;
287 Roehrs, et al. 2010; Larsen, et al. 2012; Ruedi, et al. 2013; Haynie, et al. 2016). Thus, we are confident that
288 the mitochondrial phylogeny we recovered here, and by others, reflects the true mitochondrial tree.
289 However, the mitochondrial topology may not adequately reflect the species history, particularly when
290 considering the factors that cause incongruence between nuclear and mitochondrial gene trees. Possible

291 causes of conflicting gene trees are horizontal transfer, gene duplication, introgressive hybridization, and
292 incomplete lineage sorting. Some of these phenomena are more likely to have influenced the *Myotis*
293 radiation than others.

294 Horizontal transfer of genes is thought to be rare in eukaryotes, but, vespertilionids in general
295 (Thomas, et al. 2011; Platt, et al. 2014), and *Myotis* (Pritham and Feschotte 2007; Ray, et al. 2007; Ray, et
296 al. 2008) in particular, have experienced horizontal transfer of DNA transposons. These events would not
297 be reflected in our phylogeny since repetitive sequences were removed prior to phylogenetic analyses.
298 More generally, gene duplications could create conflicting signal among individual UCE markers (ex.
299 comparing non-orthologous UCE loci), but the number of gene duplication events would have to be very
300 high to impact enough of the 3,648 UCE loci to confound the mitochondrial and nuclear phylogenies.
301 Further ruling out gene duplication events as the dominant cause of conflicting phylogenetic signal is the
302 fact that such events are likely depressed in *Myotis* as evidenced by their smaller genome size (~2.2 Gb)
303 and trend towards DNA loss (Kapusta, et al. 2017) combined with low rates of paralogy in UCEs general
304 (Derti, et al. 2006).

305 Introgressive hybridization and reticulation could significantly influence the phylogenies of *Myotis*
306 in a way that leads to conflicting signal between the nuclear and mitochondrial genomes (Sota 2002;
307 Good, et al. 2015). Hybridization in bats may be relatively common given their propensity to swarm at
308 cave entrances for breeding purposes. In European *Myotis*, swarming has allowed for high degrees of
309 hybridization between *M. brandtii*, *M. mystacinus*, and *M. alcaethoe* (Bogdanowicz, et al. 2012). Further,
310 *M. evotis*, *thysanodes*, and *keeni* all experienced historical gene flow during their divergence (Carstens
311 and Dewey 2010; Morales, et al. 2016). It is also possible to explain the differences between the
312 mitochondrial and nuclear UCE phylogenies if *Myotis* experienced extensive incomplete lineage sorting
313 during their radiation. Two factors can influence the rate of lineage sorting, the fixation rate and the
314 speciation rate (Hudson, et al. 2002). Increasing the time to fixation and/or decreasing the amount of time
315 between cladogenic events will increase the likelihood of incomplete lineage sorting. *Myotis* are generally
316 long lived species (Dzeverin 2008) and underwent a rapid radiation between 5-10 MYA (Lack, et al. 2010),
317 suggesting that *Myotis* species are likely to experience higher levels of lineage sorting. The importance of
318 these events -introgressive hybridization and incomplete lineage sorting- in driving the differences
319 between the mitochondrial and nuclear phylogenies cannot be determined with the current data.

320 **Evolutionary history of *Myotis*** – Our previous understanding of relationships within *Myotis* is
321 heavily biased with mitochondrial data because nuclear markers were harder to collect and produced
322 fewer informative sites (Ruedi and Mayer 2001; Stadelmann, et al. 2007; Lack, et al. 2010; Roehrs, et al.

2010; Larsen, et al. 2012; Ruedi, et al. 2013; Haynie, et al. 2016). Our UCE-based results indicate that nuclear trees vary substantially from the mitochondrial tree. Given that the nuclear and mitochondrial trees are different, we find it necessary to re-evaluate *Myotis* in the context of the nuclear data.

Paraphyly of *M. nigricans* and *M. albescens* was inferred from previous mitochondrial phylogenies and confirmed in the UCE tree (Larsen, et al. 2012). Larsen et al (Larsen, et al. 2012) identified a minimum of four and potentially twelve lineages in *M. albescens* and *M. nigricans*. Our sampling included four *M. albescens* and three *M. nigricans*, compared to Larsen's 17 and 29 samples. Despite different mitochondrial and nuclear topologies overall, our mitochondrial and nuclear phylogeny recovered the same paraphyletic clade of three *M. albescens* samples and *M. levis*. Close relationships between these taxa was found in previous work and expected. More importantly we did not find that *M. albescens* was paraphyletic across much of NT *Myotis*. We also found that *M. nigricans* is monophyletic in the nuclear tree, but paraphyletic in the mitochondrial tree. These results from *M. nigricans* and *M. albescens* are interesting but further inference is limited due to low sample sizes for these taxa.

The original subgeneric taxonomy of *Myotis* was based on three morphotypes that were later shown to be the result of convergent evolution (Ruedi and Mayer 2001). If lineage-sorting affected the mitochondrial phylogeny, it is possible that the morphotypes truly are monophyletic. However, superimposing the previous subgeneric/morphological classification onto the species tree shows interspersed distribution of morphotypes throughout even the most conservative nuclear tree (Figure 3). Many strongly supported terminal relationships link species with different morphotypes. Based on these results, it appears that the three major morphotypes in *Myotis* are indeed a result of convergent evolution, as suggested by previous work (Ruedi and Mayer 2001; Stadelmann, et al. 2007).

Among the more dramatic differences between the nuclear and mitochondrial topologies is the placement of *M. volans* and *M. brandtii* as sister to all New World taxa by the nuclear data. Our mitochondrial analyses place *M. volans* within a Nearctic clade and *M. brandtii* directly in-between the Nearctic and Neotropical bifurcations as has been previously reported (Stadelmann, et al. 2007). Clade probability values and bootstrap frequencies support these placements in trees from both data types. Our placement of *M. brandtii* as sister to all other New World *Myotis* more closely affiliates it with Old World taxa. This make sense given that the *M. brandtii* distribution is also Old World. On the other hand, a placement of *M. volans* sister to all New World taxa (and *M. brandtii*) in the nuclear tree is a significant departure from previous work and, at first glance, does not make as much sense in a biogeographic framework. *M. volans* is distributed across western and northwestern North America as far as far north

354 as Alaska. *M. brandtii* is distributed across much of Northern Europe. The key may lie in understanding a
355 third species, *M. gracilis*.

356 *M. gracilis*, along with *M. brandtii*, are the only two *Myotis* geographically distributed in the Old
357 World, but phylogenetically affiliated with the New World (Stadelmann, et al. 2007). If the sister
358 relationship between *M. brandtii* and *M. gracilis* (not sampled here) holds when nuclear data are
359 examined, then we can envision a scenario where *M. gracilis*, *M. brandtii*, and *M. volans* represent
360 speciation events that occurred during the transition of *Myotis* from the Old World to the New World. It
361 is important to remember that this interpretation relies on a fairly dramatic departure from the currently
362 accepted mitochondrial relationships of *M. volans* (represented here by a single sample) to other *Myotis*
363 species, and this hypothesis should be viewed as highly speculative. Increasing the number of *Myotis*
364 lineages sampled will shed additional light on this hypothesis.

365 Other taxa with conflicting positions between datasets include *M. lucifugus* + *M. occultus*, *M.*
366 *fortidens*, and *M. vivesi*. In general, these relationships are characterized by very short branches and are
367 the most likely to be affected by incomplete lineage sorting or limited phylogenetic information. This could
368 explain the strong support with the mitochondrial tree compared to the nuclear species tree, while
369 allowing for a number of nuclear loci to disagree with the species tree, as well.

370 There are a number of monophyletic groups identified with nuclear data (Fig. 1A) that exhibit
371 distinct biological characteristics. For example all of the long eared bats (*septentrionalis*, *auriculus*, *evotis*,
372 *thysanodes* and *keenii*) represent a monophyletic group of higher elevation, forest-dwelling species that
373 glean insects off of surfaces (Fitch and Shump 1979; O'Farrell and Studier 1980; Warner 1982; Manning
374 and Jones 1989; Caceres and Barclay 2000). The group represented by *fortidens*, *lucifugus* and *occultus*
375 represent a relatively long-haired form of *Myotis*. While having a distinct dental formula, *fortidens* was
376 historically described as a subspecies of *M. lucifugus* (Miller Jr and Allen 1928) and *occultus* has alternately
377 represented its own species or been considered a subspecies of *lucifugus* (Hollister 1909; Valdez, et al.
378 1999; Piaggio, et al. 2002). The clade consisting of *keaysi*, *oxyotus*, *ruber*, *simus*, *riparius*, *albescens* and
379 *diminutus* represents a NT group of primarily woolly-haired bats (LaVal 1973). If the mitochondrial
380 genome has been subjected to phenomena that obscure the true species tree then these species groups,
381 along with their synapomorphic morphological features, can be reevaluated.

382 **Conclusion** - Relationships within *Myotis*, which until now have relied heavily on mitochondrial
383 data, have served as the basis for species identification (Puechmaille, et al. 2012), evolutionary
384 hypotheses (Simões, et al. 2007), and even conservation recommendations (Boyles and Storm 2007).
385 Previous studies using nuclear data have largely been uninformative or utilized too few samples to draw

386 definitive conclusions. Trees estimated from ~3,650 nuclear loci and 295 different phylogenetic analyses
387 recovered 175 topologies, none of which are congruent with the mitochondrial phylogeny of *Myotis*.
388 Conflict between the mitochondrial and nuclear trees as well as among individual nuclear loci suggest that
389 the *Myotis* radiation may have been accompanied by high levels of incomplete lineage sorting and
390 possible hybridization. Rather than placing emphasis on the mitochondrial tree, it may be more
391 appropriate to consider it for what it really is: a single gene on par with a single UCE locus, albeit one with
392 many more phylogenetically informative characters. If true, then the mitochondrial genome is as likely to
393 reflect the true species tree as any UCE locus chosen at random. Large amounts of lineage sorting make
394 phylogenetic inference difficult and potentially impossible. Other phenomena such as reticulation,
395 hybridization, and introgression have likely influenced the genomes of *Myotis* and should be accounted
396 for in subsequent work. It is possible that the *Myotis* radiation is more accurately reflected as a hard
397 polytomy or a phylogenetic network rather than a strictly bifurcating phylogeny.

398

399 **Materials and Methods:**

400 Taxon Selection - Taxa were selected to span the major phylogenetic break points with emphasis
401 on the Nearctic and Neotropical bifurcation as recovered in previous mitochondrial phylogenies
402 (Stadelmann, et al. 2007; Ruedi, et al. 2013) (Table 1). In addition, multiple individuals morphologically
403 identified as *M. nigricans* and *M. albescens* were included to test paraphyly as demonstrated by Larsen et
404 al. (2012). Three Old World species of *Myotis* and the outgroup, *E. fuscus*, were included to root
405 phylogenetic analyses. All field identifications were confirmed from voucher specimens. Information for
406 all specimens examined is available in Table 1.

407 UCE preparation, sequencing, and processing - Genomic DNA was extracted from 33 samples
408 using either a Qiagen DNEasy extraction kit or a phenol-chloroform/ethanol precipitation. DNA was
409 fragmented using the Bioruptor UCD-300 sonication device (Diagenode, Denville, NJ, USA). Libraries were
410 prepared using the Kapa Library Preparation Kit KR0453-v2.13 (Kapa Biosystems, Wilmington, MA, USA)
411 following the manufacturer's instructions with five minor modifications. First, we used half volume
412 reactions. Second, subsequent to end repair, we added Sera-Mag Speedbeads (Thermo-Scientific,
413 Waltham, MA, USA; prepared according to (Glenn, et al. 2016)) at a ratio of 2.86:1 for end repair cleanup.
414 Third, we ligated universal iTru y-yoke adapters (Glenn, et al. 2016) onto the genomic DNA. Fourth,
415 following adapter ligation, we performed one post-ligation cleanup followed by Dual-SPRI size selection
416 using 55 μ L of speedbead buffer (22.5mM PEG, 1M NaCl) and 25 μ L of Speedbeads. Finally, we performed
417 a PCR at 95 °C for 45 sec, then 14 cycles of 98 °C for 30 sec, 60 °C for 30 sec, 72 °C for 30sec, then 72 °C

418 for a 5 minute final extension and a 12 °C hold using iTru5 and iTru7 primers to produce Illumina TruSeqHT
419 compatible libraries (Glenn, et al. 2016).

420 Libraries were quantified on a Qubit 2.0 (Life Technologies) and 83 ng from each library was added
421 to create 5 pools of 6 or 7 libraries each. We then split the pools in two. One subsample was enriched for
422 UCE loci, the other was not. UCE loci in the enriched library pools were captured using Tetrapods 5K
423 version 1 baits from MYcroarray (Ann Arbor, MI, USA) following their MYbaits protocol v. 2.3.1 with
424 overnight incubations (Faircloth, et al. 2012). Enriched libraries were quantified with a Qubit and pooled
425 with other unrelated samples prior to sequencing on an Illumina HiSeq 3000 to produce paired-end reads
426 of ≤ 151 bases. The unenriched samples were sequenced on a separate run using a single lane of Illumina
427 HiSeq 2500. All samples were demultiplexed with Illumina software fastq2bcl. Reads were quality filtered
428 by removing any potential adapter sequence and trimming read ends once the average Phred quality over
429 a four base window score dropped below 20 using the Fastx toolkit (Gordon and Hannon 2010).

430 Quality filtered raw sequence reads were assembled into contigs using the Trinity assembler
431 (Grabherr, et al. 2011) and a minimum kmer coverage of 2, and we used Phyluce to identify those
432 assembled contigs that were UCE loci. We also harvested UCE loci from *Eptesicus fuscus*
433 (GCA_000308155.1), *Myotis brandtii* (GCA_000412655.1), *M. davidii* (GCA_000327345.1), and *M.*
434 *lucifugus* (GCF_000147115.1) genome assemblies using the Phyluce package (Faircloth 2016). Once
435 extracted from Trinity and genome assemblies, we aligned all UCE loci MAFFT (Katoh, et al. 2002),
436 trimmed the aligned data with gBlocks (Castresana 2000). Repetitive sequences (i. e. transposable
437 elements) in each alignment were identified with RepeatMasker and trimmed where found.

438 Mitochondrial genome assembly and annotation – Raw reads from the unenriched libraries were
439 used to generate mitochondrial genomes via MitoBim (Hahn, et al. 2013) in most cases. This program
440 used MIRA (B, et al. 1999) to map reads to a *M. brandtii* reference genome (Genbank accession number
441 KT210199.1). Alternative methods of mitochondrial genome assembly were used when MitoBim assembly
442 failed. These taxa include *M. albescens* (TK61766), *M. albescens* (TK 101723), *M. albescens* (RDS 7889), *M.*
443 *fortidens*, *M. keeni*, *M. melanorhinus*, *M. nigricans* (QCAZ 9601), *M. septentrionalis*, *M. simus*, *M. velifer*,
444 and *M. volans*. For these samples, we first identified reads that were mitochondrial in origin using BLAST
445 searches against the *M. brandtii* mitochondrial genome (KT210199.1). Those reads were assembled using
446 Trinity v2.2.0 with the –single option. For taxa where we either could not assemble useable mitochondrial
447 genomes, we retrieved proxy data from GenBank as follows: *M. brandtii* (KT210199.1), *E. fuscus*
448 (KF111725.1), *M. lucifugus* (KP273591.1), and *M. davidii* (KM233172.1).

449 Once assembled, each mitogenome was annotated via MITOS (Bernt, et al. 2013). Annotated
450 genes were manually validated via BLAST to confirm sequence identity and length. Protein coding genes
451 were checked for stop codons using EMBOSS's transeq program (Rice, et al. 2000). When a stop codon
452 was found, we used the raw reads to verify the sequence. We used BWA v0.7.12 (Li and Durbin 2009) to
453 align the reads to the Mitobim assembled mitogenome to verify base calls from Mitobim. The protein
454 coding rRNA and tRNA genes from each assembly were aligned using MUSCLE and concatenated into a
455 single alignment for phylogenetic analyses, as described below.

456 Initial phylogenetic analyses - Initial phylogenies derived from UCE loci and mitochondrial coding
457 regions were generated using maximum likelihood and Bayesian methodologies. For the first round of
458 phylogenetic analyses all UCE loci present in 20 or more taxa were concatenated into a single alignment.
459 PartitionFinder v1.1.1 (Lanfear, et al. 2012) was used to identify and combine loci into an optimal
460 partitioning scheme using the hcluster heuristic algorithm. We assumed a GTR+ Γ model for all loci (Darriba
461 and Posada 2015). Initial trees were generated using RAxML v7.4.1 (Stamatakis 2006) with linked branch
462 lengths RaxML (v8.1.3) was used to estimate and score the maximum likelihood phylogeny with the rapid
463 bootstrapping option and 1,000 bootstrap replicates. We define strongly supported bipartitions as those
464 present in 95-100% of bootstrap replicates and moderately supported bipartitions are present in 85-95%
465 of bipartitions (Wiens, et al. 2008). A Bayesian phylogeny was generated with the MPI version of ExaBayes
466 (v1.4.1) using two independent runs of 4 chains each. ExaBayes runs were terminated after 1 million
467 generations only if the average standard deviation of split frequencies was less than 0.01. The first 25% of
468 samples were discarded after which every 100th generation was sampled. The "-M 3" option was used to
469 reduce the memory footprint of all ExaBayes runs. Proper sampling, post burn-in was inspected via Tracer
470 v1.6. (Rambaut, et al. 2014). Effective sample sizes greater than 200 were considered acceptable.
471 Posterior probability values greater than 95% were considered to be significant.

472 The mitochondrial phylogeny was generated using methods similar to those described above with
473 the following exceptions. All 37 coding regions, including protein coding genes, tRNA and rRNAs, were
474 concatenated into a single alignment. Genes were partitioned individually except in the instances where
475 two genes overlapped. These regions were partitioned separately from the individual genes resulting in
476 three partitions for the two genes: a partition for gene A, a partition for gene B, and a partition for the
477 overlapping nucleotides of gene A and B. The fast bootstrapping search in RAxML was run for 10K
478 replicates and Bayesian analyses were performed across four independent runs with four chains of ten
479 million generations.

480 The mitochondrial and nuclear phylogenies were compared to each other to identify discordance
481 between marker types. Site-log likelihood scores were calculated for the mitochondrial alignments when
482 constrained to the nuclear tree while the nuclear alignment was scored against the mitochondrial tree
483 using RAxML. Model parameters were then recalculated for each constrained alignment (-f G). Site-log
484 likelihood scores were analyzed using CONSEL (Shimodaira and Hasegawa 2001) and compared using the
485 approximately unbiased test (Shimodaira 2002). P-values less than 0.05 were used to indicate that the
486 trees produced by mitochondrial or nuclear data differed.

487 *Extended phylogenetic analyses* - Many factors can influence phylogenetic inference. To reduce
488 the likelihood of any single factor influencing the results, we re-examined the nuclear UCE dataset using
489 the strategies described below. A flow chart of analyses is available in Supplemental Figure 1.

490 Aligned UCE loci were binned based on the number of taxa represented in the alignment
491 (phyluce_align_get_only_loci_with_min_taxa; Faircloth 2016), or degree of completeness. Groups
492 included loci present in 100% (number of specimens (n) = 37), 95% (n = 35), 85% (n = 31), 75% (n = 27),
493 65% (n = 24), 55% (n = 20), 45% (n = 16), 35% (n = 12), 25% (n = 9), and 15% (n = 5) of specimens examined.
494 These 10 groups were non-exclusive, so a locus that was assembled in all specimens (100% complete)
495 would also be included with loci present in only 55% of specimens. On the other hand, a locus found in
496 only 55% of specimens would not be included in the 100% complete data set. Each set of UCE alignments
497 was concatenated using phyluce_align_format_nexus_files_for_raxml and a nexus character block was
498 created using the phyluce_align_format_nexus_files_for_raxml -charsets option. These datasets then
499 served as the basis for downstream phylogenetic analyses. For example, when a partitioning methodology
500 (discussed below) was tested, it was performed for each of the 100%, 95%, 85%, etc. alignments. In
501 addition to partitioning schemes, the effect of missing data was examined using Bayesian and maximum
502 likelihood methods.

503 Concatenated alignments were analyzed using three different partitioning schemes.
504 Unpartitioned alignments were simply concatenated UCE loci treated as a single genetic unit (No
505 Partitions). Fully partitioned alignments were concatenated alignments of UCE loci that were partitioned
506 by locus (All Partitions). Finally, PartitionFinder v1.1.1 (Lanfear, et al. 2012) was used to combine individual
507 loci into an optimal partitioning scheme (Optimal Partitions). Rather than searching for best-fit
508 substitution models for each UCE locus or partition, the GTR+ Γ model of sequence evolution was assigned
509 to all loci (Darriba and Posada 2015). Initial trees for PartitionFinder were generated using RAxML v7.4.1
510 (Stamatakis 2006) with linked branch lengths. Partitioning schemes were heuristically searched using the
511 hcluster algorithm.

512 Maximum likelihood trees were inferred for the concatenated alignments using RAxML v8.1.3
513 (Stamatakis 2014). The three partitioning schemes (described above) were applied to each analysis. The
514 best scoring (lowest -lnL) tree from each dataset was identified from 100 random starting trees and
515 bootstrapped 100 times using the GTR+ Γ in both cases. The autoMRE function in RAxML v8.1.3 was used
516 to determine the need for additional bootstrap replicates beyond the initial 100 (Pattengale, et al. 2009).
517 A stopping criterion was set *a priori* if the weighted Robinson-Foulds distance was less than 5% in 95% of
518 random permutations of computed bootstrap replicates (Pattengale, et al. 2009). If necessary, an
519 additional 100 bootstrap replicates were computed until the convergence stopping criteria were met.
520 Finally, bipartition frequencies of bootstrap replicates were drawn onto the best scoring tree from the
521 initial RAxML searches for each of the respective data sets.

522 Bayesian analyses were conducted using ExaBayes v1.4.1 (Aberer, et al. 2014). For all Bayesian
523 analyses four independent runs of four chains each were run in parallel for a minimum of one hundred
524 thousand generations sampling every thousandth generation and applying a GTR+ Γ substitution model
525 for each partition. Two of the partitioning schemes (described above) were used for each analysis: No
526 Partitions and Optimal Partitions. After one hundred thousand generations, analyses continued until the
527 standard deviation of the split frequency between chains was less than 0.01. An extended majority rule
528 consensus tree was created from all trees after the first 25% of trees were discarded using TreeAnnotator
529 v1.7.0 (Rambaut and Drummond 2013) and parameter estimates across all runs were calculated with
530 Tracer v1.6 (Rambaut, et al. 2014).

531 *Sampling loci by number of informative characters* – Previous coalescent analyses of UCE data
532 have shown that sub-sampling the most informative loci can result in different topologies (Meiklejohn, et
533 al. 2016). Under these assumptions, UCE loci were sorted into ten groups based on their length and the
534 predicted correlation between length and number of informative characters was confirmed
535 (Supplemental Figure 2). UCE loci in the same size cohort were combined into a single alignment. Rather
536 than using coalescent based analyses we used concatenation of UCE loci to identify different topologies
537 based on length. UCE loci were individually partitioned and the maximum likelihood tree was estimated
538 with the rapid bootstrapping option in RaxML (bootstrap replicates = 100) using the GTR+ Γ substitution
539 model.

540 *Random sampling of loci* – In large phylogenetic analyses, systematic error can result in highly
541 supported, but incorrect topologies as a result of compounding non-phylogenetic signal (Rodríguez-
542 Ezpeleta, et al. 2007). By randomly reducing the dataset and replicating the ML analyses, we can reduce
543 the potential effects of compounding error. Roughly 10% of the dataset, 365 loci, were randomly sampled

544 and concatenated to create 100 new alignments. ML methods were similar to those used when sampling
545 loci by the number of informative characters.

546 *Summary methods* – Gene trees for individual UCE loci recovered in five or more taxa were
547 inferred using the GTR+ Γ substitution model and fast bootstrapping (-f a) option in RAxML (replicates =
548 1,000). In general, gene trees were classified based on the degree of completeness (i.e. number of taxa
549 represented) similar to the way we treated individuals as described above.

550 Species trees were estimated and bootstrapped using three different programs. ASTRAL-II v4.10
551 (Mirarab and Warnow 2015) was used to build a summary tree. Support values for bipartitions in the tree
552 were generated from 100 bootstrap replicates using site as well as site and locus resampling (Seo 2008).
553 Species trees were estimated from ASTRID v1.4 (Vachaspati and Warnow 2015) using bionj and
554 bootstrapped for 100 replicates. SVDquartets (Chifman and Kubatko 2014), as implemented in PAUP
555 v4.0a150 (Swofford 2003), was used to estimate a species trees from a random subset of 200,000 quartets
556 and 1,000 bootstrap replicates.

557 Errors in gene tree estimation may reduce the accuracy of summary methods (Liu, et al. 2009;
558 Leaché and Rannala 2011; DeGiorgio and Degnan 2014; Mirarab, et al. 2016). We used weighted (Bayzid,
559 et al. 2015) and unweighted (Mirarab, et al. 2014) statistical binning to combine gene trees into
560 compatible supergenes using the pipeline available in Bayzid et al. (Bayzid, et al. 2015). The gene trees
561 used for the summary tree methods described above were used rather than re-estimating trees.
562 Bifurcations supported by more than 50% of the bootstrap replicates were retained for each gene tree.
563 Alignments from compatible trees were concatenated into a single supergene alignment. Trees for
564 supergenes were estimated using RAxML. The best trees for each supergene, as defined by log likelihood
565 score, were retained from 500 searches. Bipartition support was estimated from 500 bootstrap replicates.
566 For all analyses, the GTR+ Γ model of substitution was used and each gene in the supergene alignment was
567 partitioned separately. The resulting supertrees were then used for species tree estimation using ASTRAL-
568 II. For the unweighted analysis, all supertrees were included in the pool of trees. For the weighted analysis,
569 supertrees were weighted according to the number of genes combined in the supergene alignment. For
570 example, if a supergene was a composite of six genes, the supertree was present 6 times compared to a
571 composite of five genes which would be represented only five times. Support for the weighted and
572 unweighted species trees was estimated by site and site and locus re-sampling (Seo 2008) for 100
573 bootstrap replicates in ASTRAL-II.

574 *Meta-analyses* - Trees recovered from all analyses were compared to each other in tree space.
575 Unweighted Robinson-Foulds distances were calculated among all trees. This distance matrix was

576 transformed into two dimensions using the stochastic CCA algorithm for nonlinear dimension reduction
577 in TreeScaper v1.09 (Huang, et al. 2016). Coordinates were then visualized in R using hexagonal binning
578 in the hexbin library v1.27.1 (Lewin-Koh 2011).

579 We compared the mitochondrial data to all nuclear trees. Branch lengths have different meanings
580 based on the type of analysis. For example, ASTRAL-II branch lengths are representative of coalescent
581 units. ASTRID doesn't even calculate branch lengths. For accurate tree comparisons, branch lengths were
582 stripped from all trees using regular expressions and Sed. Site log-likelihood scores were calculated for
583 each nuclear tree, without branch lengths, and using the mitochondrial alignment. Model parameters
584 were re-estimated for each tree. Site-log likelihood scores were compared with the approximately
585 unbiased (Shimodaira 2002) and Shimodaira-Hasegawa (Shimodaira and Hasegawa 1999) test in CONSEL
586 and values less than 0.05 were indicative of differences. Finally, we used RAxML to generate a 85% and
587 majority rule consensus trees from all nuclear trees.

588

589 **Acknowledgments:**

590 We would like to thank the following museums, collection managers, and collaborators for the
591 tissue loans necessary to complete this work: Joseph Cook (Museum of Southwestern Biology), Museum
592 of Vertebrate Zoology, Manuel Ruedi (Natural History Museum of Geneva), Santiago Burneo (Pontificia
593 Universidad Catolica del Ecuador Museo de Zoologia), Heath Garner, Robert Bradley and Caleb Phillips
594 (Texas Tech University Natural Science Research Laboratory), Link Olson (University of Alaska Museum of
595 the North), Cody Thompson and Priscilla Tucker (University of Michigan Museum of Zoology). In addition,
596 we would like to thank the Texas Tech HPCC (www.hpcc.ttu.edu) for providing the computational
597 resources necessary to complete this project. This work was supported by the National Science
598 Foundation, DEB-1355176. Additional support was provided by College of Arts and Sciences at Texas Tech
599 University. All sequence data is available at NCBI's Short Read Archive (SRP095250). UCE contig assemblies
600 are available at (PENDING ACCESSION NUMBER). Supplemental files include: a nexus file containing all
601 estimated species trees (AllTrees.nex), an archived file of individual UCE alignments in fasta format
602 (uceLociAlignments.tgz), and an archived file containing all individual UCE gene trees in newick format
603 (UceGeneTrees.tgz).

604

605 **Figure and Table Captions**

606 **Figure 1.** Comparison of nuclear and mitochondrial phylogenetic trees in *Myotis*. Bayesian trees
607 generated from (A) 2,890 nuclear UCE loci and (B) 37 mitochondrial protein, tRNA, and rRNA genes (B)
608 Posterior probability values greater than 0.95 are shown as a “*”. Values below branches are
609 percentages of maximum likelihood bootstrap replicates supporting that clade. Conflicting tips between
610 data types (nuclear vs. mitochondrial) are indicated with lines between the topologies. The
611 mitochondrial Bayesian and maximum likelihood trees resolved different relationships among *M.*
612 *thysanodes*, *evotis*, and *keeni* as indicated by the dotted lines. Species with more than one sample are
613 designated with a superscript that is referenced in Table 1. Specimens derived from whole genome
614 alignments are designated with a superscript “G”.

615 **Figure 2.** Differences between mitochondrial and nuclear topologies. (A) All trees recovered from
616 mitochondrial genes and the extended analysis of the nuclear data were visualized in tree space using
617 multidimensional scaling. Nuclear trees (green) were distinct from mitochondrial trees forming a large
618 cluster. Most nuclear trees were found within a limited region of tree space. Mitochondrial trees (blue)
619 were distinct from any of the 294 nuclear trees recovered. Tree vs tree comparisons show that most (B)
620 nuclear trees are more similar to each other than they are to (C) mitochondrial trees. Symmetric
621 differences are equal to twice the Robinson-Foulds distance between two trees.

622 **Figure 3.** Consensus tree. A consensus tree of New World *Myotis* was generated from 294 nuclear
623 topologies with a threshold cutoff of 85%. Values shown above the branches represent the percentage
624 of nuclear analyses that support a given bipartion. Previous subgeneric classifications based on
625 morphology are listed at each tip (*Myotis* “M”, *Selysius* “S”, *Leuconoe* “L”. Biogeographic regions are
626 color coded. Species with more than one sample are designated with a superscript that is referenced in
627 Table 1. Specimens derived from whole genome alignments are designated with a superscript “G”. This
628 consensus tree represents a very conservative estimate of the *Myotis* radiation.

629 **Table 1.** Specimens examined.

630 Collection abbreviations: Museum of Southwestern Biology (MSB), Museum of Vertebrate Zoology
631 (MVZ), Natural History Museum of Geneva (MHNG), Pontificia Universidad Catolica del Ecuador Museo
632 de Zoologia (QCAZ), Texas Tech University Natural Science Research Laboratory (TK), University of Alaska
633 Museum of the North (UAM), University of Michigan Museum of Zoology (UMMZ)

634 **Table 2.** General alignment information. For a subset of analyses a series of alignments were generated
635 based on the number of taxa per locus. Thirty-seven taxa were examined so an alignment with all 37
636 taxa was considered 100% complete. Parsimony-informative characters make up a small portion of the
637 total alignment. The optimum partitioning scheme was calculated with PartitionFinder.

638 **Sup Fig 1.** Analytical flow chart. In the initial analysis (A) mitochondrial and nuclear data were analyzed
639 using Bayesian and maximum likelihood methods. Trees were compared using the approximately
640 unbiased and the Shimodaira-Hasegawa tests and determined to be conflicting. Extended analysis (B) of
641 the data used multiple methods and sampling strategies to generate 292 different phylogenetic
642 inferences. (C) All nuclear and mitochondrial trees were compared in tree space and with topological
643 tests. An 85% meta-consensus tree from all analyses was used to represent a conservative estimate of
644 the *Myotis* radiation. Trees from the extended analysis were compared to the mitochondrial trees using
645 the approximately unbiased and the Shimodaira-Hasegawa tests and determined to be conflicting.

646 **Sup Fig 2.** UCE loci sorted by length. The length of a UCE locus is correlated with the number of
647 phylogenetically informative characters. UCE loci were sorted by length and ten bins of alignments were
648 created so that the shortest loci were combined into one alignment, the next shortest set of loci were
649 combined ... etc. Parsimony informative characters made up a minor part of each alignment.

650 **Sup Table 1.** Tree topology tests. Trees were compared to each other using the approximately unbiased
651 and the Shimodaira-Hasegawa tests. Likelihood scores were calculated for the mitochondrial alignment
652 when constrained to all topologies (mitochondrial and nuclear) recovered herein. Alignment and tree
653 topology incompatibility were identified as p-values < 0.01.

654 **Sup File -AllTrees.nex** – Trees generated from all analyses in nexus format.

655 **Sup File -uceLociAlignments.tgz** – Fasta alignments of all UCE loci recovered in at least four taxa.

656 **Sup File -UceGeneTrees.tgz** – UCE gene trees for all loci recovered in at least four taxa. Trees were
657 inferred from 100 ML searches using RAxML.

658 **Literature Cited**

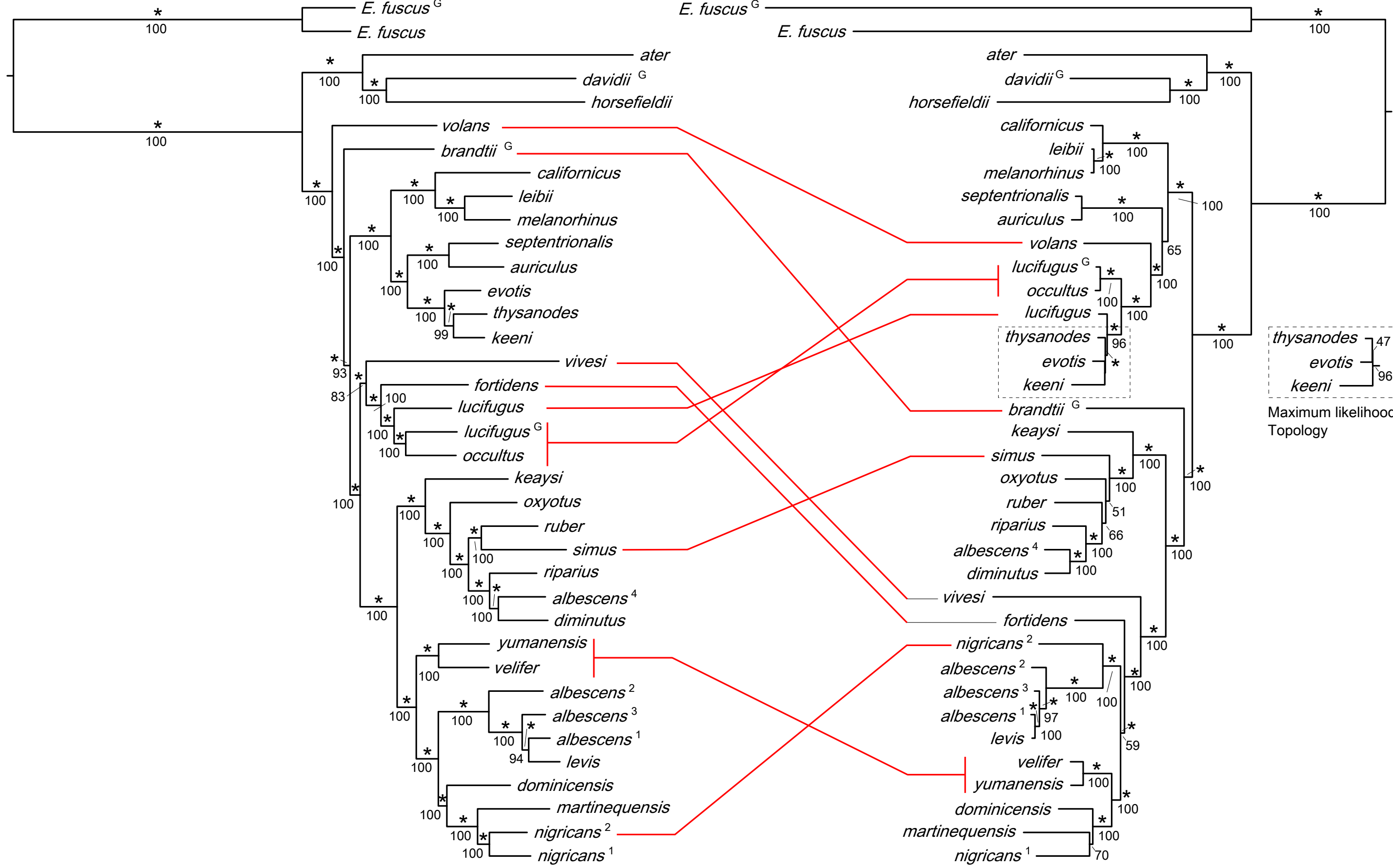
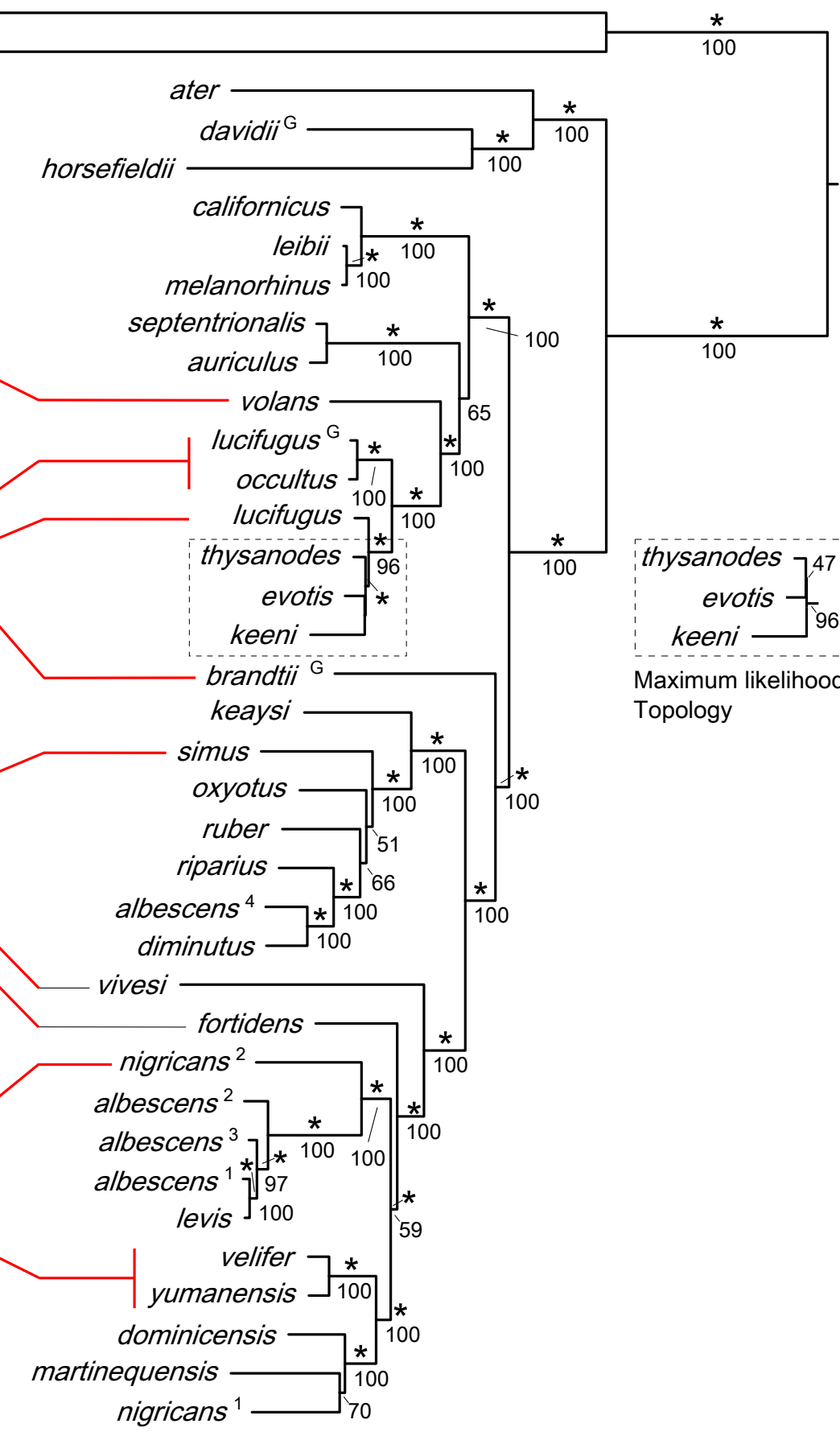
- 659 Aberer AJ, Kobert K, Stamatakis A. 2014. ExaBayes: Massively parallel Bayesian tree inference for the
660 whole-genome era. *Molecular Biology and Evolution* 31:2553-2556.
- 661 Genome sequence assembly using trace signals and additional sequence information [Internet]. 1999 1
662 August 2015]. Available from: <http://www.bioinfo.de/isb/gcb99/talks/chevreux/main.html>
- 663 Bayzid MS, Mirarab S, Boussau B, Warnow T. 2015. Weighted statistical binning: Enabling statistically
664 consistent genome-scale phylogenetic analyses. *PLoS ONE* 10:e0129183.
- 665 Bernt M, Donath A, Jühling F, Externbrink F, Florentz C, Fritzsch G, Pütz J, Middendorf M, Stadler PF.
666 2013. MITOS: Improved de novo metazoan mitochondrial genome annotation. *Molecular*
667 *Phylogenetics and Evolution* 69:313-319.
- 668 Bogdanowicz W, Piksa K, Tereba A. 2012. Hybridization hotspots at bat swarming sites. *PLoS ONE*
669 7:e53334.
- 670 Boyles JG, Storm JJ. 2007. The perils of picky eating: Dietary breadth is related to extinction risk in
671 insectivorous bats. *PLoS ONE* 2:e672.
- 672 Caceres MC, Barclay RMR. 2000. *Myotis septentrionalis*. *Mammalian Species*:1-4.
- 673 Carstens BC, Dewey TA. 2010. Species delimitation using a combined coalescent and information-
674 theoretic approach: An example from North American *Myotis* bats. *Systematic Biology* 59:400-414.
- 675 Castresana J. 2000. Selection of conserved blocks from multiple alignments for their use in phylogenetic
676 analysis. *Molecular Biology and Evolution* 17:540-552.
- 677 Chifman J, Kubatko L. 2014. Quartet inference from SNP data under the coalescent model.
678 *Bioinformatics* 30:3317-3324.
- 679 Crawford NG, Faircloth BC, McCormack JE, Brumfield RT, Winker K, Glenn TC. 2012. More than 1000
680 ultraconserved elements provide evidence that turtles are the sister group of archosaurs. *Biology*
681 *Letters* 8:783-786.
- 682 Darriba D, Posada D. 2015. The impact of partitioning on phylogenomic accuracy.
- 683 DeGiorgio M, Degnan JH. 2014. Robustness to divergence time underestimation when inferring species
684 trees from estimated gene trees. *Systematic Biology* 63:66-82.
- 685 Degnan JH, Rosenberg NA. 2009. Gene tree discordance, phylogenetic inference and the multispecies
686 coalescent. *Trends in Ecology & Evolution* 24:332-340.
- 687 Derti A, Roth FP, Church GM, Wu Ct. 2006. Mammalian ultraconserved elements are strongly depleted
688 among segmental duplications and copy number variants. *Nat Genet* 38:1216-1220.
- 689 Douady CJ, Delsuc F, Boucher Y, Doolittle WF, Douzery EJP. 2003. Comparison of Bayesian and maximum
690 likelihood bootstrap measures of phylogenetic reliability. *Molecular Biology and Evolution* 20:248-254.
- 691 Dzeverin I. 2008. The stasis and possible patterns of selection in evolution of a group of related species
692 from the bat genus *Myotis* (Chiroptera, Vespertilionidae). *Journal of Mammalian Evolution* 15:123-
693 142.
- 694 Edwards S, Bensch S. 2009. Looking forwards or looking backwards in avian phylogeography? A
695 comment on Zink and Carrowclough 2008. *Molecular Ecology* 18:2930-2933.
- 696 Faircloth BC. 2016. PHYLUCE is a software package for the analysis of conserved genomic loci.
697 *Bioinformatics* 32:786-788.
- 698 Faircloth BC, Branstetter MG, White ND, Brady SG. 2015. Target enrichment of ultraconserved elements
699 from arthropods provides a genomic perspective on relationships among Hymenoptera. *Molecular*
700 *Ecology Resources* 15:489-501.
- 701 Faircloth BC, McCormack JE, Crawford NG, Harvey MG, Brumfield RT, Glenn TC. 2012. Ultraconserved
702 elements anchor thousands of genetic markers spanning multiple evolutionary timescales. *Systematic*
703 *Biology*:sys004.
- 704 Findley JS. 1972. Phenetic relationships among bats of the genus *Myotis*. *Systematic Biology* 21:31-52.

- 705 Fitch JH, Shump KA. 1979. *Myotis keenii*. Mammalian Species Archive 121:1-3.
- 706 Glenn TC, Nilsen R, Kieran TJ, Finger JW, Pierson TW, Bentley KE, Hoffberg S, Louha S, Garcia-De-Leon FJ,
707 Angel del Rio Portilla M, et al. 2016. Adapterama I: Universal stubs and primers for thousands of dual-
708 indexed Illumina libraries (iTru & iNext). bioRxiv.
- 709 Good JM, Vanderpool D, Keeble S, Bi K. 2015. Negligible nuclear introgression despite complete
710 mitochondrial capture between two species of chipmunks. *Evolution* 69:1961-1972.
- 711 Gordon A, Hannon G. 2010. Fastx-toolkit. http://hannonlab.cshl.edu/fastx_toolkit.
- 712 Grabherr MG, Haas BJ, Yassour M, Levin JZ, Thompson DA, Amit I, Adiconis X, Fan L, Raychowdhury R,
713 Zeng Q, et al. 2011. Full-length transcriptome assembly from RNA-Seq data without a reference
714 genome. *Nat Biotech* 29:644-652.
- 715 Green RE, Braun EL, Armstrong J, Earl D, Nguyen N, Hickey G, Vandewege MW, St. John JA, Capella-
716 Gutiérrez S, Castoe TA, et al. 2014. Three crocodylian genomes reveal ancestral patterns of evolution
717 among archosaurs. *Science* 346.
- 718 Hahn C, Bachmann L, Chevreux B. 2013. Reconstructing mitochondrial genomes directly from genomic
719 next-generation sequencing reads—a baiting and iterative mapping approach. *Nucleic Acids Research*
720 41:e129.
- 721 Haynie ML, Tsuchiya MTN, Ospina-Garcés SM, Arroyo-Cabrales J, Medellín RA, Polaco OJ, Maldonado JE.
722 2016. Placement of the rediscovered *Myotis planiceps* (Chiroptera: Vespertilionidae) within the *Myotis*
723 phylogeny. *Journal of Mammalogy* 97:701-712.
- 724 Hedtke SM, Townsend TM, Hillis DM. 2006. Resolution of phylogenetic conflict in large data sets by
725 increased taxon sampling. *Systematic Biology* 55:522-529.
- 726 Hollister N. 1909. Two new bats from the southwestern United States: publisher not identified.
- 727 Hosner PA, Faircloth BC, Glenn TC, Braun EL, Kimball RT. 2016. Avoiding missing data biases in
728 phylogenomic inference: An empirical study in the landfowl (Aves: Galliformes). *Molecular Biology and*
729 *Evolution* 33:1110-1125.
- 730 Huang H, He Q, Kubatko LS, Knowles LL. 2010. Sources of error inherent in species-tree estimation:
731 Impact of mutational and coalescent effects on accuracy and implications for choosing among
732 different methods. *Systematic Biology* 59:573-583.
- 733 Huang W, Zhou G, Marchand M, Ash JR, Morris D, Van Dooren P, Brown JM, Gallivan KA, Wilgenbusch
734 JC. 2016. TreeScaper: Visualizing and extracting phylogenetic signal from sets of trees. *Molecular*
735 *Biology and Evolution*.
- 736 Hudson RR, Coyne JA, Huelsenbeck J. 2002. Mathematical consequences of the genealogical species
737 concept. *Evolution* 56:1557-1565.
- 738 Kapusta A, Suh A, Feschotte C. 2017. Dynamics of genome size evolution in birds and mammals.
739 *Proceedings of the National Academy of Sciences* 114:E1460-E1469.
- 740 Katoh K, Misawa K, Kuma Ki, Miyata T. 2002. MAFFT: a novel method for rapid multiple sequence
741 alignment based on fast Fourier transform. *Nucleic Acids Research* 30:3059-3066.
- 742 Lack JB, Roehrs ZP, Stanley CE, Ruedi M, Van Den Bussche RA. 2010. Molecular phylogenetics of *Myotis*
743 indicate familial-level divergence for the genus *Cistugo* (Chiroptera). *Journal of Mammalogy* 91:976-
744 992.
- 745 Lanfear R, Calcott B, Ho SYW, Guindon S. 2012. PartitionFinder: Combined selection of partitioning
746 schemes and substitution models for phylogenetic analyses. *Molecular Biology and Evolution* 29:1695-
747 1701.
- 748 Larsen RJ, Knapp MC, Genoways HH, Khan FAA, Larsen PA, Wilson DE, Baker RJ. 2012. Genetic diversity
749 of neotropical *Myotis* (Chiroptera: Vespertilionidae) with an emphasis on South American species.
750 *PLoS ONE* 7:e46578.
- 751 LaVal RK. 1973. A revision of the Neotropical bats of the genus *Myotis*: Natural History Museum, Los
752 Angeles County.

- 753 Leaché AD, Rannala B. 2011. The accuracy of species tree estimation under simulation: A comparison of
754 methods. *Systematic Biology* 60:126-137.
- 755 Leavitt DH, Marion AB, Hollingsworth BD, Reeder TW. 2017. Multilocus phylogeny of alligator lizards
756 (Elgaria, Anguidae): Testing mtDNA introgression as the source of discordant molecular phylogenetic
757 hypotheses. *Molecular Phylogenetics and Evolution*.
- 758 Lewin-Koh N. 2011. Hexagon binning: an overview.
759 ftp://ftp.naist.jp/pub/lang/R/CRAN/web/packages/hexbin/vignettes/hexagon_binning.pdf.
- 760 Li G, Davis BW, Eizirik E, Murphy WJ. 2016. Phylogenomic evidence for ancient hybridization in the
761 genomes of living cats (Felidae). *Genome Research* 26:1-11.
- 762 Li H, Durbin R. 2009. Fast and accurate short read alignment with Burrows–Wheeler transform.
763 *Bioinformatics* 25:1754-1760.
- 764 Liu L, Yu L, Kubatko L, Pearl DK, Edwards SV. 2009. Coalescent methods for estimating phylogenetic
765 trees. *Molecular Phylogenetics and Evolution* 53:320-328.
- 766 Maddison WP, Knowles LL. 2006. Inferring phylogeny despite incomplete lineage sorting. *Systematic
767 Biology* 55:21-30.
- 768 Manning RW, Jones JK. 1989. *Myotis evotis*. *Mammalian Species Archive* 329:1-5.
- 769 McCormack JE, Harvey MG, Faircloth BC, Crawford NG, Glenn TC, Brumfield RT. 2013. A Phylogeny of
770 birds based on over 1,500 loci collected by target enrichment and high-throughput sequencing. *PLoS
771 ONE* 8:e54848.
- 772 McGee MD, Faircloth BC, Borstein SR, Zheng J, Darrin Hulsey C, Wainwright PC, Alfaro ME. 2016.
773 Replicated divergence in cichlid radiations mirrors a major vertebrate innovation. *Proceedings of the
774 Royal Society B: Biological Sciences* 283.
- 775 Meiklejohn KA, Faircloth BC, Glenn TC, Kimball RT, Braun EL. 2016. Analysis of a rapid evolutionary
776 radiation using Ultraconserved Elements: Evidence for a bias in some multispecies coalescent
777 methods. *Systematic Biology* 65:612-627.
- 778 Miller Jr GS, Allen G. 1928. The American bats of the genus *Myotis* and *Pixonyx*. *Bulletin of the United
779 States National Museum* 144:1-218.
- 780 Mirarab S, Bayzid MS, Boussau B, Warnow T. 2014. Statistical binning enables an accurate coalescent-
781 based estimation of the avian tree. *Science* 346.
- 782 Mirarab S, Bayzid MS, Warnow T. 2016. Evaluating summary methods for multilocus species tree
783 estimation in the presence of incomplete lineage sorting. *Systematic Biology* 65:366-380.
- 784 Mirarab S, Warnow T. 2015. ASTRAL-II: Coalescent-based species tree estimation with many hundreds of
785 taxa and thousands of genes. *Bioinformatics* 31:i44-i52.
- 786 Morales AE, Jackson ND, Dewey TA, O’Meara BC, Carstens BC. 2016. Speciation with gene flow in North
787 American *Myotis* bats. *Systematic Biology*.
- 788 O’Farrell MJ, Studier EH. 1980. *Myotis thysanodes*. *Mammalian Species* 137:1-5.
- 789 Pattengale ND, Alipour M, Bininda-Emonds ORP, Moret BME, Stamatakis A. 2009. How many bootstrap
790 replicates are necessary? In: Batzoglou S, editor. *Research in Computational Molecular Biology: 13th
791 Annual International Conference, RECOMB 2009, Tucson, AZ, USA, May 18-21, 2009. Proceedings.*
792 Berlin, Heidelberg: Springer Berlin Heidelberg. p. 184-200.
- 793 Piaggio AJ, Valdez EW, Bogan MA, Spicer GS. 2002. Systematics of *Myotis occultus* (Chiroptera:
794 Vespertilionidae) inferred from sequences of two mitochondrial genes. *Journal of Mammalogy* 83:386-
795 395.
- 796 Platt RN, Vandewege MW, Kern C, Schmidt CJ, Hoffmann FG, Ray DA. 2014. Large numbers of novel
797 miRNAs originate from DNA transposons and are coincident with a large species radiation in bats.
798 *Molecular Biology and Evolution* 31:1536-1545.

- 799 Platt RN, Zhang Y, Witherspoon DJ, Xing J, Suh A, Keith MS, Jorde LB, Stevens RD, Ray DA. 2015. Targeted
800 capture of phylogenetically informative Ves SINE Insertions in genus *Myotis*. *Genome Biology and*
801 *Evolution* 7:1664-1675.
- 802 Pritham EJ, Feschotte C. 2007. Massive amplification of rolling-circle transposons in the lineage of the
803 bat *Myotis lucifugus*. *Proceedings of the National Academy of Sciences* 104:1895-1900.
- 804 Puechmaille SJ, Allegrini B, Boston ESM, Dubourg-Savage M-J, Evin A, Knochel A, Le Bris Y, Lecoq V,
805 Lemaire M, Rist D, et al. 2012. Genetic analyses reveal further cryptic lineages within the *Myotis*
806 *nattereri* species complex. *Mammalian Biology* 77:224-228.
- 807 Rambaut A, Drummond A. 2013. TreeAnnotator v1. 7.0.
- 808 Rambaut A, Suchard M, Xie D, Drummond A. 2014. Tracer v1.6.
- 809 Ray DA, Feschotte C, Pagan HJT, Smith JD, Pritham EJ, Arensburger P, Atkinson PW, Craig NL. 2008.
810 Multiple waves of recent DNA transposon activity in the bat, *Myotis lucifugus*. *Genome Research*
811 18:717-728.
- 812 Ray DA, Pagan HJT, Thompson ML, Stevens RD. 2007. Bats with hATs: Evidence for recent DNA
813 transposon activity in genus *Myotis*. *Molecular Biology and Evolution* 24:632-639.
- 814 Rice P, Longden I, Bleasby A. 2000. EMBOSS: the European molecular biology open software suite. In:
815 Elsevier Current Trends.
- 816 Rodríguez-Ezpeleta N, Brinkmann H, Roure B, Lartillot N, Lang BF, Philippe H. 2007. Detecting and
817 overcoming systematic errors in genome-scale phylogenies. *Systematic Biology* 56:389-399.
- 818 Roehrs ZP, Lack JB, Van Den Bussche RA. 2010. Tribal phylogenetic relationships within Vespertilioninae
819 (Chiroptera: Vespertilionidae) based on mitochondrial and nuclear sequence data. *Journal of*
820 *Mammalogy* 91:1073-1092.
- 821 Ruedi M, Mayer F. 2001. Molecular systematics of bats of the genus *Myotis* (Vespertilionidae) suggests
822 deterministic ecomorphological convergences. *Molecular Phylogenetics and Evolution* 21:436-448.
- 823 Ruedi M, Stadelmann B, Gager Y, Douzery EJP, Francis CM, Lin L-K, Guillén-Servent A, Cibois A. 2013.
824 Molecular phylogenetic reconstructions identify East Asia as the cradle for the evolution of the
825 cosmopolitan genus *Myotis* (Mammalia, Chiroptera). *Molecular Phylogenetics and Evolution* 69:437-
826 449.
- 827 Sanderson MJ, Shaffer HB. 2002. Troubleshooting molecular phylogenetic analyses. *Annual Review of*
828 *Ecology and Systematics* 33:49-72.
- 829 Seo T-K. 2008. Calculating bootstrap probabilities of phylogeny using multilocus sequence data.
830 *Molecular Biology and Evolution* 25:960-971.
- 831 Shimodaira H. 2002. An Approximately Unbiased test of phylogenetic tree selection. *Systematic Biology*
832 51:492-508.
- 833 Shimodaira H, Hasegawa M. 2001. CONSEL: For assessing the confidence of phylogenetic tree selection.
834 *Bioinformatics* 17:1246-1247.
- 835 Shimodaira H, Hasegawa M. 1999. Multiple comparisons of log-likelihoods with applications to
836 phylogenetic inference. *Molecular Biology and Evolution* 16:1114.
- 837 Simmons NB. 2005. Order Chiroptera. *Mammal species of the world: a taxonomic and geographic*
838 *reference* 1:312-529.
- 839 Simões BF, Rebelo H, Lopes RJ, Alves PC, Harris DJ. 2007. Patterns of genetic diversity within and
840 between *Myotis d. daubentonii* and *M. d. nathalinae* derived from cytochrome *b* mtDNA sequence
841 data. *Acta Chiropterologica* 9:379-389.
- 842 Sota T. (Sota2002 co-authors). 2002. Radiation and reticulation: extensive introgressive hybridization in
843 the carabid beetles *Ohomopterus* inferred from mitochondrial gene genealogy. *Population Ecology*
844 44:0145-0156.

- 845 Stadelmann B, Lin LK, Kunz TH, Ruedi M. 2007. Molecular phylogeny of New World *Myotis* (Chiroptera,
846 Vespertilionidae) inferred from mitochondrial and nuclear DNA genes. *Molecular Phylogenetics and*
847 *Evolution* 43:32-48.
- 848 Stamatakis A. 2006. RAxML-VI-HPC: maximum likelihood-based phylogenetic analyses with thousands of
849 taxa and mixed models. *Bioinformatics* 22:2688-2690.
- 850 Stamatakis A. 2014. RAxML version 8: A tool for phylogenetic analysis and post-analysis of large
851 phylogenies. *Bioinformatics* 30:1312-1313.
- 852 Swofford DL. 2003. PAUP*. Phylogenetic analysis using parsimony (* and other methods). Version 4.
- 853 Thomas J, Sorourian M, Ray D, Baker RJ, Pritham EJ. 2011. The limited distribution of Helitrons to vesper
854 bats supports horizontal transfer. *Gene* 474:52-58.
- 855 Vachaspati P, Warnow T. (Vachaspati2015 co-authors). 2015. ASTRID: Accurate Species TRees from
856 Internode Distances. *BMC Genomics* 16:S3.
- 857 Valdez EW, Choate JR, Bogan MA, Yates TL. 1999. Taxonomic status of *Myotis occultus*. *Journal of*
858 *Mammalogy* 80:545-552.
- 859 Warner RM. 1982. *Myotis auriculus*. *Mammalian Species* 191:1-3.
- 860 Wiens JJ, Kuczynski CA, Smith SA, Mulcahy DG, Sites JJW, Townsend TM, Reeder TW. 2008. Branch
861 lengths, support, and congruence: Testing the phylogenomic approach with 20 nuclear loci in snakes.
862 *Systematic Biology* 57:420-431.
- 863 Willis SC, Farias IP, Ortí G. 2014. Testing mitochondrial capture and deep coalescence in Amazonian
864 cichlid fishes (Cichlidae: *Cichla*). *Evolution* 68:256-268.
- 865

A**B**

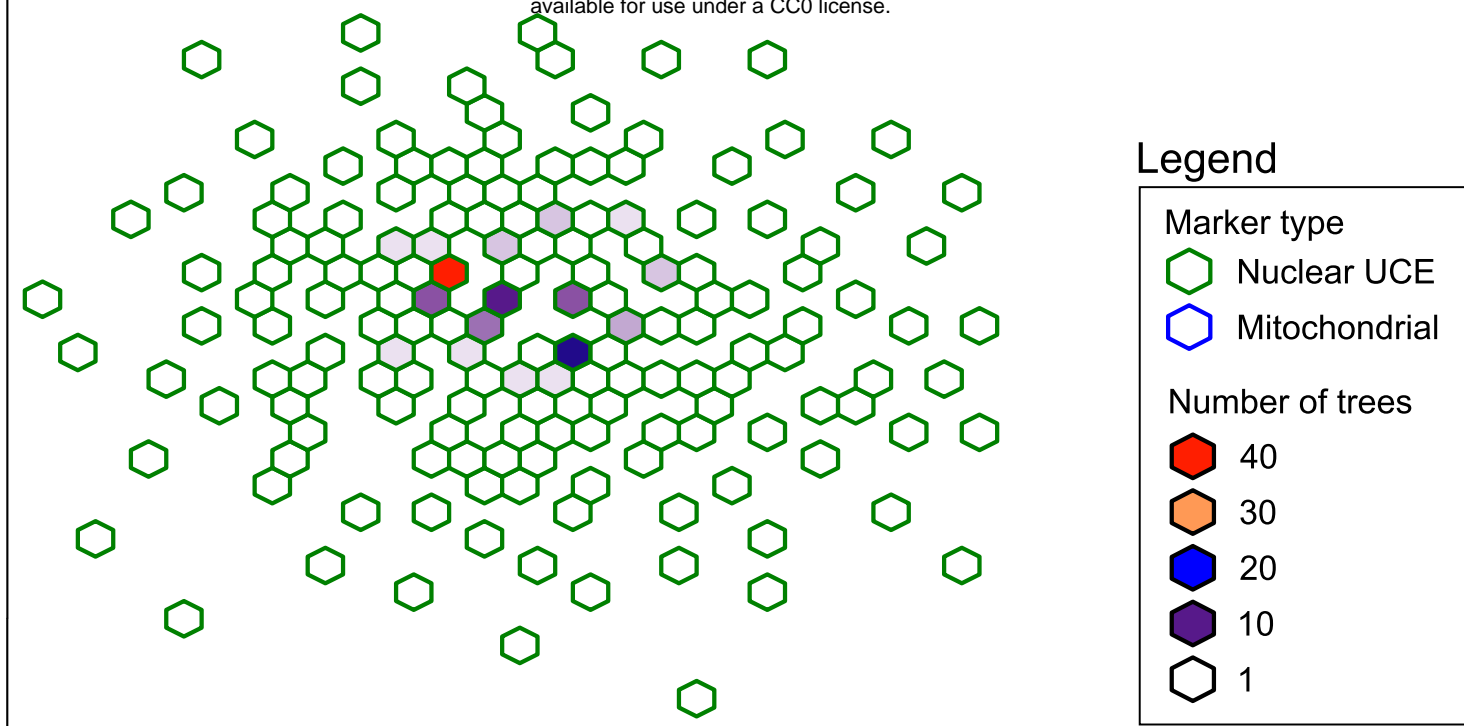
0.003

0.08

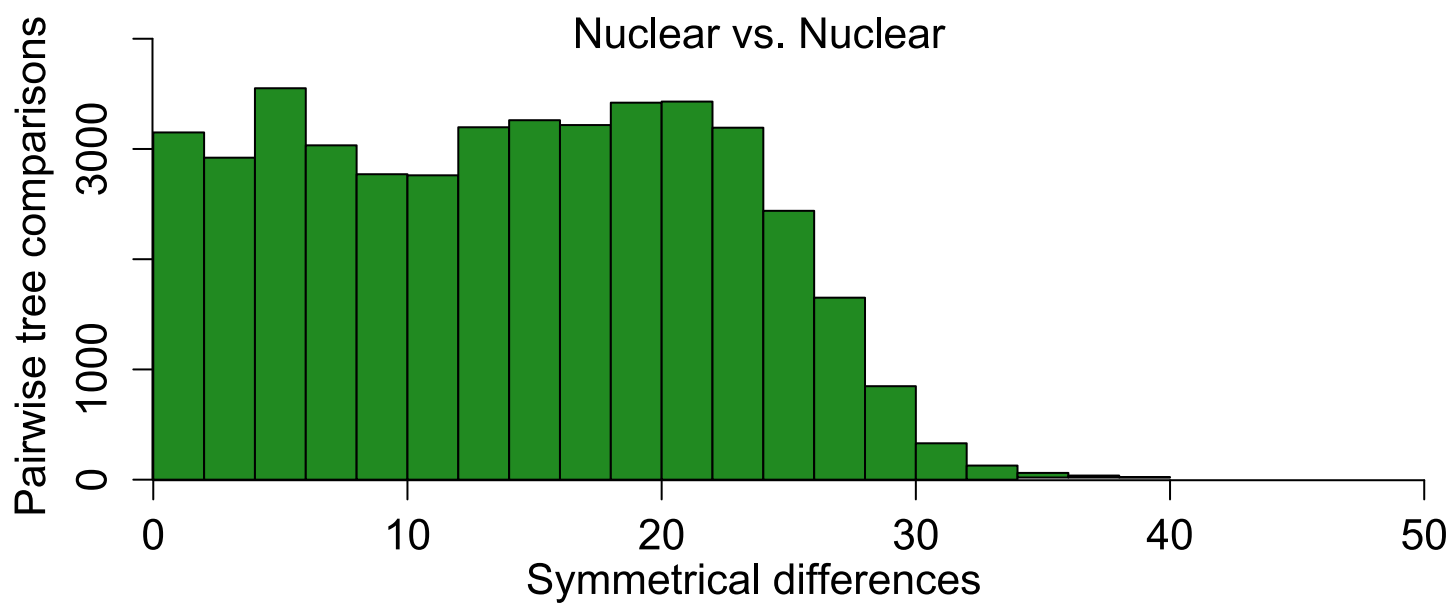
A



bioRxiv preprint first posted online Feb. 28, 2017; doi: <http://dx.doi.org/10.1101/112581>. The copyright holder for this preprint (which was not peer-reviewed) is the author/funder. This article is a US Government work. It is not subject to copyright under 17 USC 105 and is also made available for use under a CC0 license.



B



C

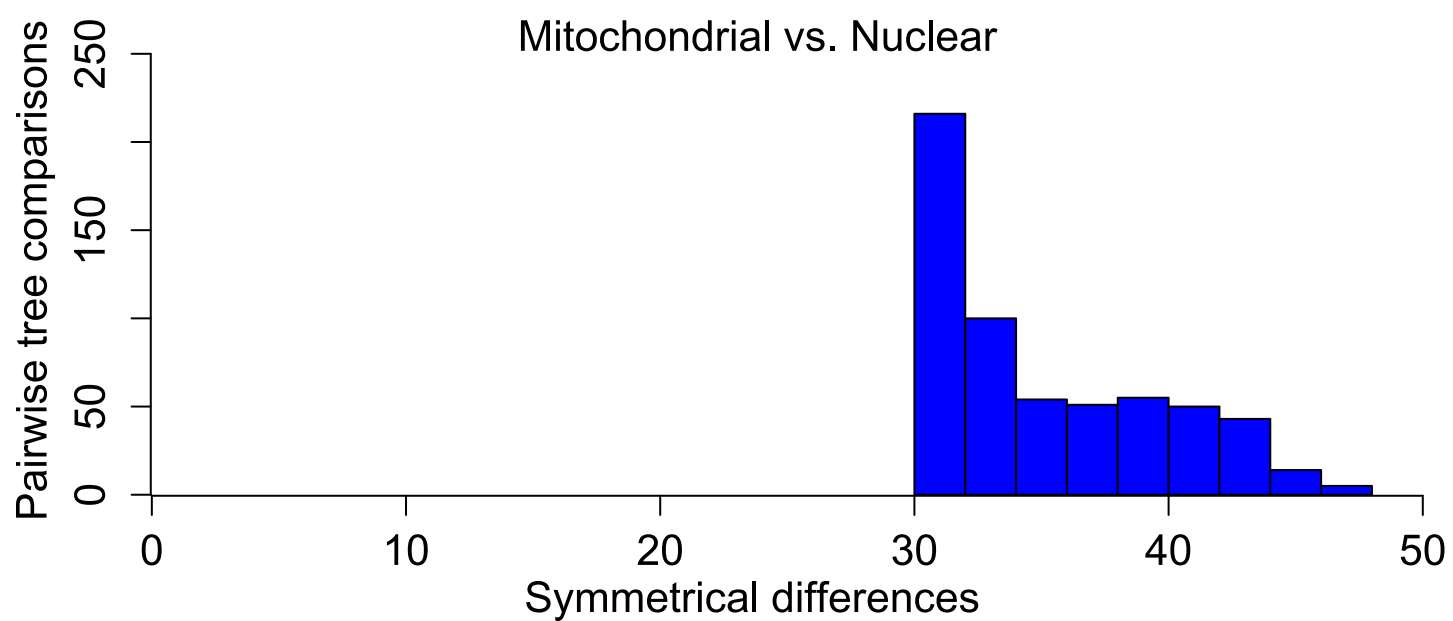


Table 1 - Specimens Examined

Genus	Specific epithet	Name herein	Museum identification num.	Num. UCE Loci	UCE contig accession	Mitochondrial genome accession
<i>Eptesicus</i>	<i>fuscus</i>	<i>fuscus</i>	TK 178736	2,849	Pending	Pending
<i>Eptesicus</i>	<i>fuscus</i>	<i>fuscus</i> ^G	GCA_000308155.1	2,467	Pending	Pending
<i>Myotis</i>	<i>albescens</i>	<i>albescens</i> ¹	RDS 7889	2,764	Pending	Pending
<i>Myotis</i>	<i>albescens</i>	<i>albescens</i> ²	QCAZ 9157	1,185	Pending	Pending
<i>Myotis</i>	<i>albescens</i>	<i>albescens</i> ³	TK 61766	2,872	Pending	Pending
<i>Myotis</i>	<i>albescens</i>	<i>albescens</i> ⁴	TK 101723	2,990	Pending	Pending
<i>Myotis</i>	<i>atacamensis</i>	<i>atacamensis</i>	M4430	2,774	Pending	Pending
<i>Myotis</i>	<i>auriculus</i>	<i>auriculus</i>	MSB 40883	2,229	Pending	Pending
<i>Myotis</i>	<i>brandtii</i>	<i>brandtii</i> ^G	GCA_000412655.1	2,446	Pending	Pending
<i>Myotis</i>	<i>septentrionalis</i>	<i>septentrionalis</i>	RDS 7705	2,916	Pending	Pending
<i>Myotis</i>	<i>californicus</i>	<i>californicus</i>	UMMZ 175828	2,948	Pending	Pending
<i>Myotis</i>	<i>davidii</i>	<i>davidii</i> ^G	GCA_000327345.1	2,450	Pending	Pending
<i>Myotis</i>	<i>dominicensis</i>	<i>dominicensis</i>	TK 15624	2,576	Pending	Pending
<i>Myotis</i>	<i>evotis</i>	<i>evotis</i>	MSB 47323	2,586	Pending	Pending
<i>Myotis</i>	<i>fortidens</i>	<i>fortidens</i>	MSB 54941	2,791	Pending	Pending
<i>Myotis</i>	<i>horsfieldii</i>	<i>horsefeldii</i>	MHNG 1926.039	3,017	Pending	Pending
<i>Myotis</i>	<i>keaysi</i>	<i>keaysi</i>	TK 13525	3,195	Pending	Pending
<i>Myotis</i>	<i>keenii</i>	<i>keenii</i>	UAM 113849	2,723	Pending	Pending
<i>Myotis</i>	<i>leibii</i>	<i>leibii</i>	TK 24872	3,119	Pending	Pending
<i>Myotis</i>	<i>levis</i>	<i>levis</i>	RDS 7781	2,538	Pending	Pending
<i>Myotis</i>	<i>lucifugus</i>	<i>lucifugus</i>	MSB 46679	2,736	Pending	Pending
<i>Myotis</i>	<i>lucifugus</i>	<i>lucifugus</i> ^G	GCA_000147115.1	2,429	Pending	Pending
<i>Myotis</i>	<i>martiniquensis</i>	<i>martiniquensis</i>	TK 151413	856	Pending	Pending
<i>Myotis</i>	<i>melanorhinus</i>	<i>melanorhinus</i>	M8944	3,177	Pending	Pending
<i>Myotis</i>	<i>nigricans</i>	<i>nigricans</i> ¹	QCAZ 9601	2,854	Pending	Pending
<i>Myotis</i>	<i>nigricans</i>	<i>nigricans</i> ²	RDS 7791	3,159	Pending	Pending
<i>Myotis</i>	<i>nigricans</i> or <i>diminutus</i>	<i>nigricans</i> ³	QCAZ 9168	3,078	Pending	Pending
<i>Myotis</i>	<i>occultus</i>	<i>occultus</i>	MSB 121995	2,957	Pending	Pending
<i>Myotis</i>	<i>oxyotus</i>	<i>oxyotus</i>	UMMZ RCO1013	3,106	Pending	Pending
<i>Myotis</i>	<i>riparius</i>	<i>riparius</i>	TK 145199	2,890	Pending	Pending
<i>Myotis</i>	<i>ruber</i>	<i>ruber</i>	MVZ 185692	2,757	Pending	Pending
<i>Myotis</i>	<i>simus</i>	<i>simus</i>	TK 22688	2,924	Pending	Pending
<i>Myotis</i>	<i>thysanodes</i>	<i>thysanodes</i>	07LEP	2,821	Pending	Pending
<i>Myotis</i>	<i>velifer</i>	<i>velifer</i>	MSB 70877	2,704	Pending	Pending
<i>Myotis</i>	<i>vivesi</i>	<i>vivesi</i>	MSB 42658	2,469	Pending	Pending
<i>Myotis</i>	<i>volans</i>	<i>volans</i>	MSB 40886	2,819	Pending	Pending
<i>Myotis</i>	<i>yumanensis</i>	<i>yumanensis</i>	RDS 7734	2,589	Pending	Pending

Collection abbreviations: Museum of Southwestern Biology (MSB), Museum of Vertebrate Zoology (MVZ), Natural History Museum of Geneva (MHNG), Pontificia Universidad Catolica del Ecuador Museo de Zoologia (QCAZ), Texas Tech University Natural Science Research Laboratory (TK), University of Alaska Museum of the North (UAM), University of Michigan Museum of Zoology (UMMZ). Samples beginning with "GCA_" represent genome assemblies available through NCBI. 

Table 2. Character information

Min. num. of taxa	Percent of taxa per locus	Number of Loci	Parsimony-informative characters	Variable uninformative	Alignment length	Optimum Partitions
37	100	212	3,480	4,778	112,125	6
35	95	1,193	18,288	24,189	575,321	15
31	85	2,034	29,179	41,711	903,903	16
27	75	2,481	33,031	48,732	1,041,099	20
24	65	2,668	34,373	51,148	1,091,620	27
20	55	2,890	35,284	53,200	1,144,471	27
16	45	3,064	36,539	54,782	1,187,492	31
12	35	3,232	37,259	56,453	1,227,093	34
9	25	3,379	37,894	57,672	1,260,248	37
5	15	3,648	38,718	62,588	1,377,262	31

General alignment information. For a subset of analyses a series of alignments were generated based on the number of taxa per locus. Thirty-seven taxa were examined so an alignment with all 37 taxa was considered 100% complete. Parsimony-informative characters make up a small portion of the total alignment. The optimum partitioning scheme was calculated with PartitionFinder.